

LTCC DIFFERENTIAL-FED PATCH ANTENNAS WITH RAT-RACE FEEDING STRUCTURES

K.-S. Chin^{*}, J.-A. Liu, C.-C. Chang, and J.-C. Cheng

Chang Gung University, Taoyuan 333, Taiwan, R.O.C.

Abstract—This paper presents differential-fed patch antennas with excellent cross-polarization. This paper provides a detailed graphic illustration of factors that lead to deteriorated H -plane cross-polarization by the conventional single-ended feeding probes. A novel differential rat-race feeding structure was constructed to allow easy impedance matching. An experimental antenna was realized on low-temperature co-fired ceramic (LTCC) at 8 GHz. An excellent cross-polarization of less than -22.5 dB was achieved. When the operation frequency is high, the parasitic inductance caused by feeding probes may degrade the performance of antennas. This paper further proposes the use of differential aperture-coupled structures at high frequencies. An aperture-coupled antenna realized at 40 GHz with low cross-polarization < -15 dB has been achieved.

1. INTRODUCTION

Differential microwave circuits have recently become popular for their harmonic suppression, low noise, and high linearity. Differential patch antennas not only integrate easily with ready-made differential devices, but can also improve cross-polarization significantly.

Researchers have proposed various approaches for differential patch antennas [1–5, 7–12]. Petosa et al. [1] demonstrated the feasibility of using dual feeding probes with out-of-phase currents to suppress unwanted radiation from the probe. However, factors causing deterioration in H -plane cross-polarization and E -plane co-polarization are not well explained. Researchers recently developed an accurate cavity model for differentially driven microstrip antennas [2] to analyze their input impedance and radiation characteristics. Only antennas operating at low frequencies were fabricated and measured.

Received 18 July 2012, Accepted 16 August 2012, Scheduled 22 August 2012

* Corresponding author: Kuo-Sheng Chin (kschin@mail.cgu.edu.tw).

In [3], cross-shaped slots were cut on a patch to separate the two differential feeding probes. This design requires a Wilkinson power divider and a 180° delay line leading to bulky circuits. Antennas designed with meandering half-wavelength feeding strips were proposed in [4]. The currents at the vertical segments of strips have a 180° phase shift, canceling the leakage radiation from the feeding strip. Instead of feeding the patch directly, the design in [5] fed an H-shaped aperture on the ground plane by differential probes to couple energy to the stacked patches. This design also included more metal layers and a complex structure. Both proximity coupling and aperture coupling are non-contact feeding techniques in patch antennas [6–8, 11, 12]. Lee et al. [7] proposed a differential proximity-coupled structure for integrating an active antenna with a discrete push-pull power amplifier. Because this design places a differential feeding circuit on the same side as the patches, it may produce undesired front radiations if it cannot be incorporated into the differential amplifier. [8] presented differential aperture-coupled patch antennas using two ground apertures coupled to a balanced feed. An extra patch element placed behind the feed line to effectively block the back radiation acted as a reflector.

This paper presents differential-fed patch antennas with low cross-polarization at frequencies up to 40 GHz. A differential rat-race feeding structure was constructed to allow easy impedance matching. This study also proposes a differential aperture-coupled structure to reduce the parasitic inductance caused by feeding probes at high frequencies. Two experimental LTCC antennas were demonstrated with excellent cross-polarization.

2. DIFFERENTIAL FEEDING CIRCUITS

Figure 1(a) shows a conventional probe-fed patch antenna connected to an opposite-side input microstrip. The upper substrate with a low dielectric constant can promote radiation. A lower substrate containing the microstrip line can have a high dielectric constant to enhance the fields of feed lines. Placing the input microstrip on the opposite side can avoid undesired front radiation. However, the feeding probe is unbalanced (single-ended) because of its different current paths through the probe and the ground plane. This causes undesired radiation and increases the level of cross-polarization. Fig. 1(b) shows the current distribution of the single-ended probe-fed patch antenna, while the ground plane is removed for clarity. The probe's current acts roughly like a short dipole, and contributes significantly to the interferential patterns shown in Fig. 1(c). This situation becomes worse as the probe length increases, greatly increasing the level of H -plane cross-polarization.

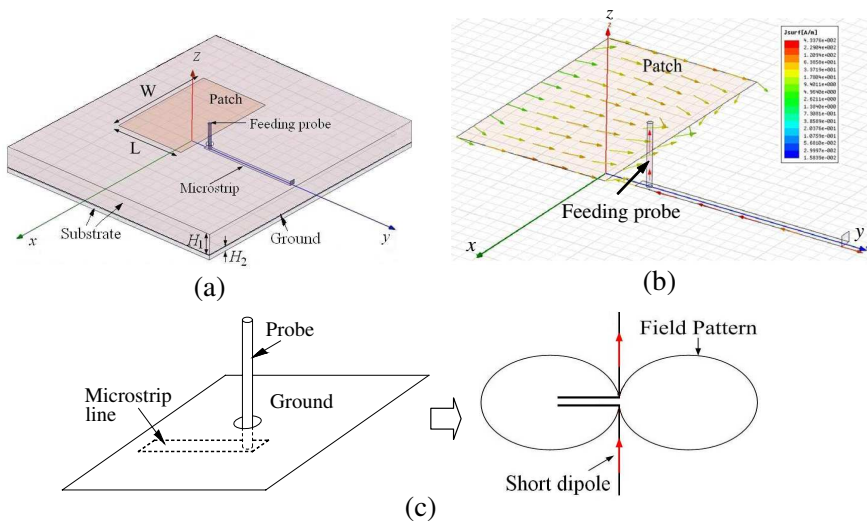


Figure 1. (a) Conventional probe-fed patch antenna. (b) Current distribution of the probe-fed patch antenna (with the ground plane removed for clarity). (c) Interferential pattern caused by the feeding probe.

Figure 2 provides a detailed graphic illustration of factors that lead to deteriorated E -plane co-polarization and H -plane cross-polarization of using the conventional single-ended feeding probes. In the case of E -plane co-polarization shown in Fig. 2(a), the electric fields of the transmitting horn and the patch antenna are both co-polarized, as denoted by the arrow E . The radiation pattern is measured by rotating the receiving patch antenna in its E -field direction. The probe current gradually orients toward the E -field direction of the horn as the rotation angle approaches 90° to make the probe behave as a short dipole and cause interferential patterns. The influence is usually not serious because the probe's current is small compared with the patch current. For suspended and thick-substrate patch antennas, the radiation from long probes contributes greatly to the E -plane co-polarization, causing asymmetric patterns [1]. Fig. 2(b) illustrates the H -plane cross-polarized pattern test by crossing the magnetic fields of the patch and the horn. The pattern is measured by rotating the receiving patch in its H -field direction. The probe current gradually becomes co-polarized with the horn as the rotation angle approaches 90° , whereas the patch is cross-polarized with the horn. Consequently, the probe current significantly degrades the performance of H -plane cross-polarization. The middle of Figs. 2(a) and 2(b) provides graphical illustrations of the pattern superposition.

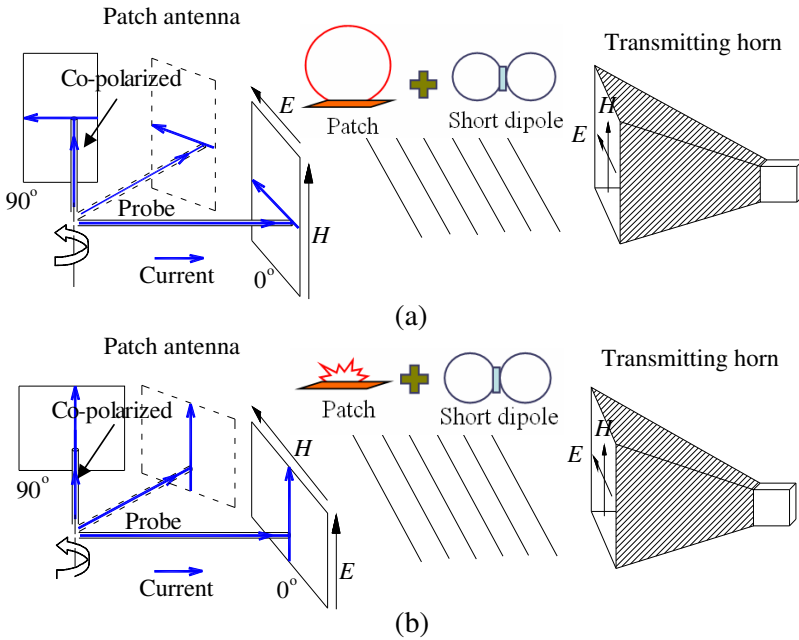


Figure 2. Illustration of (a) E -plane co-polarized and (b) H -plane cross-polarized radiation pattern measurements for single-ended probed patch antennas.

This paper proposes a novel rat-race feeding patch antenna with low cross-polarization. Fig. 3(a) plots the 3D schematic of the proposed antenna. Two out-of-phase probes from the rat-race go through the ground aperture to excite the patch differentially. Fig. 3(b) plots the schematic of the proposed differential feeding circuit, where Ports 2 and 3 denote the differential output ports. The proposed differential feeding structure is modified from the conventional rat-race, of which the isolated port is removed. Adding two shunt open-circuited stubs symmetrically at a distance from the output ports achieves impedance matching. Such an impedance tuning design is convenient from a circuit integration aspect, because it does not require lumped elements. Fig. 3(c) indicates the patch antenna driven differentially at positions of $(x_1, y_1) = (0.5W, 0.1L)$ and $(x_2, y_2) = (0.5W, 0.9L)$ with $L_1 = 0.8L$ to excite the TM_{10} mode. Compared with the single-ended antenna, the differentially-driven patch antenna has larger resonant resistance, increasing the difficulty of impedance matching [2]. A larger L_1 is generally preferred for lower matching impedance and higher radiation efficiency.

In a conventional rat-race, the isolated port is designed to isolate

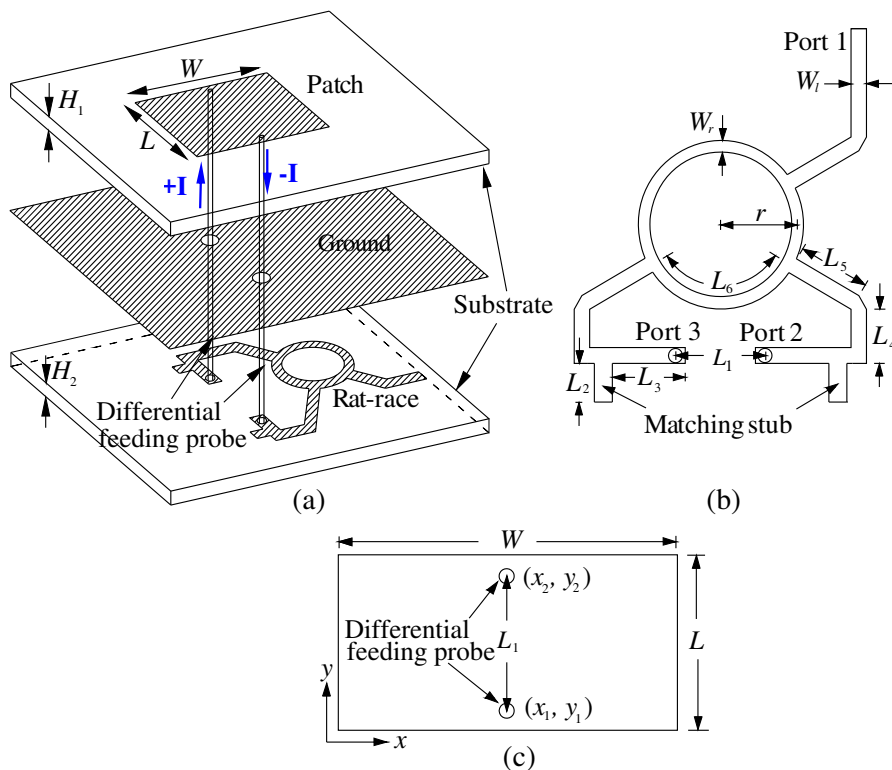


Figure 3. (a) 3D schematic of the proposed differential probe-fed patch antenna. (b) The proposed rat-race feeding circuit. (c) Feeding position on the patch.

output ports, preventing interference from each other. However, the isolated port must be terminated with an internal or external matched load (typically $50\ \Omega$), which is not cost effective and difficult to realize especially at high frequencies. Thus, it is helpful to remove the isolated port. Considering the effects caused by remove of isolated ports, the S -parameter responses of the rat-race was studied in detail. Figs. 4(a) and 4(b) show the simulated S -parameter and phase responses of the rat-race (with $\epsilon_r = 4.3$, $\tan \delta = 0.02$, and $H = 0.762\ \text{mm}$) without an isolated port at 5.8 GHz. Results reserving isolated ports are also included for comparison. If the isolated port is omitted, $|S_{21}| = -4.24\ \text{dB}$ and $|S_{31}| = -4.21\ \text{dB}$ still achieve equal power split and out-off-phase ($\angle S_{21} = -57^\circ$ and $\angle S_{31} = 123^\circ$). Both without and with the isolated ports exhibit similar S_{11} performances, but S_{23} is degraded from $-28.7\ \text{dB}$ (with) to $-13.46\ \text{dB}$ (without). The radiation patterns with/without the isolated port were studied to analyze the

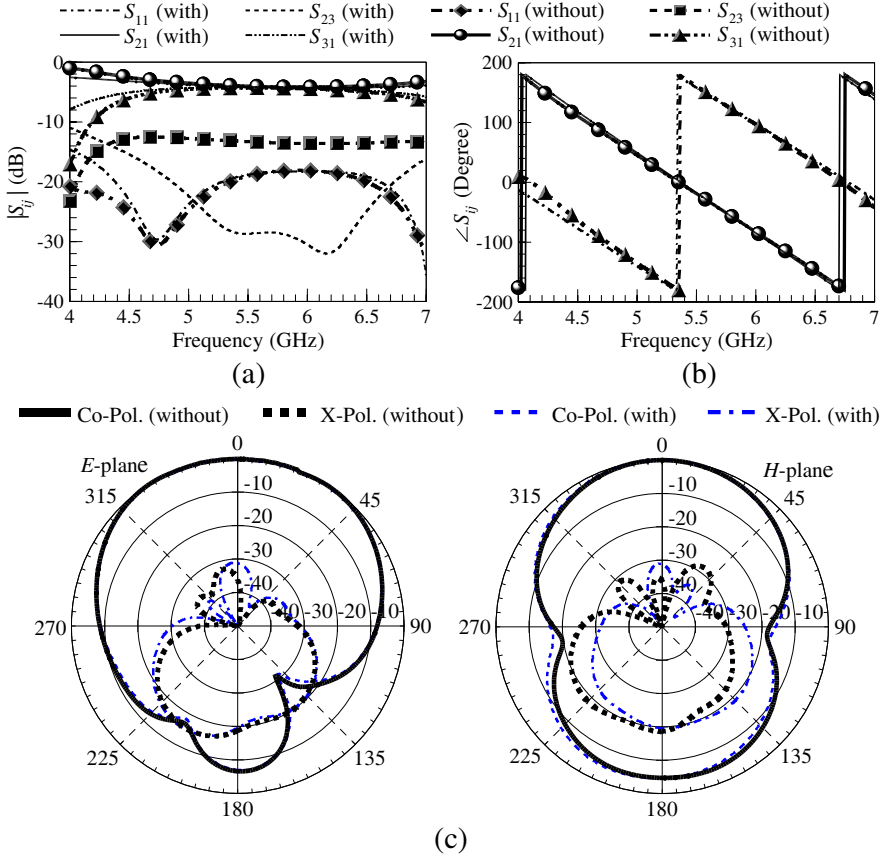


Figure 4. (a) S -parameter responses of the rat-race. (b) Phase of the rat-race. (c) Radiation patterns of the differential antenna without and with isolated ports.

effect caused by degraded S_{23} . Fortunately, the simulated radiation patterns of the 5.8-GHz antenna show only slight variation between the without and with isolated ports in Fig. 4(c). This is because of the balanced feeding structure and symmetric feeding position. Therefore, removing the isolated port simplifies the design.

A probe-fed patch antenna with stub-loaded feeding circuits can be modeled using a shunt capacitor in series with an inductor loaded with a RLC resonator (patch). The capacitance and inductance respectively represent the effect of matching stubs and feeding probes on the input impedance of patch antennas. Fig. 3(b) shows that the adjustable parameters for impedance matching are the stub distance L_3 and the stub length L_2 . To qualitatively analyze the matching

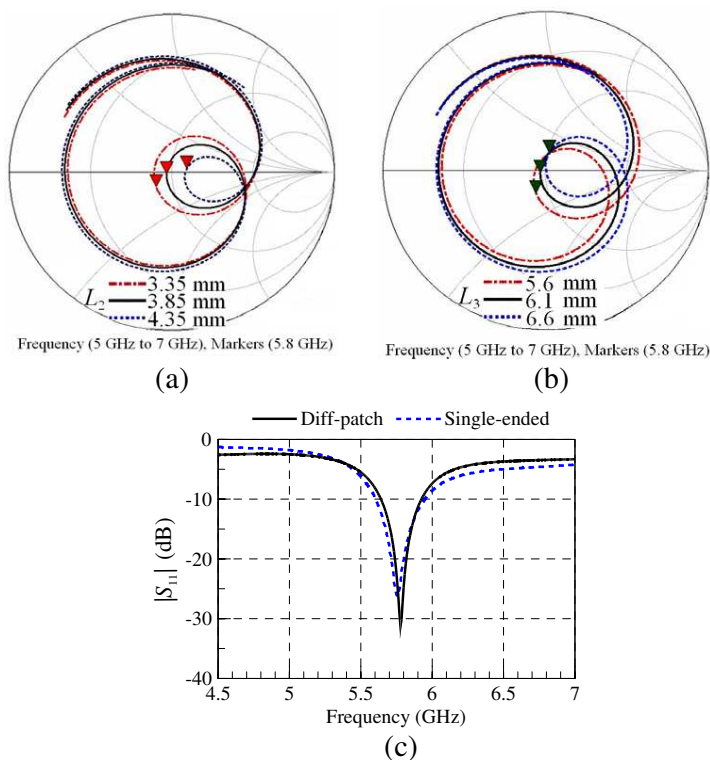


Figure 5. (a) Smith charts with varied L_2 . (b) Smith charts with varied L_3 . (c) S_{11} responses for antennas with the proposed differential and the conventional single-ended feeding structures.

behavior of the stub-loaded feeding circuit and therefore its design, Fig. 5 shows the Smith charts of the differential antenna by tuning L_2 and L_3 . Because a short open-circuited stub is equivalent to a shunt capacitance, the input impedance is more capacitive if a shorter L_2 is chosen (with fixed $L_3 = 6.1$ mm) as the mark ∇ of Fig. 5(a) shows. However, the input impedance becomes more inductive in Fig. 5(b) if a longer L_3 is designed (with fixed $L_2 = 3.85$ mm) because of an increase in series inductance. An excellent impedance matched condition of 50Ω can be achieved by choosing the proper combination of L_2 and L_3 . Bandwidth comparison of antennas with the proposed differential and the conventional single-ended feeding structures was conducted. Fig. 5(c) shows the differential and single-ended feeding structures for a 5.8-GHz patch antenna possessing almost the same simulated S_{11} curves and bandwidths.

3. DIFFERENTIAL PROBE-FED AND APERTURE-COUPLED PATCH ANTENNAS

3.1. Differential Probe-fed Patch Antenna

An 8-GHz LTCC differential probe-fed antenna, Antenna I, was designed using the structure shown in Fig. 3 with $W = 9.09$ mm,

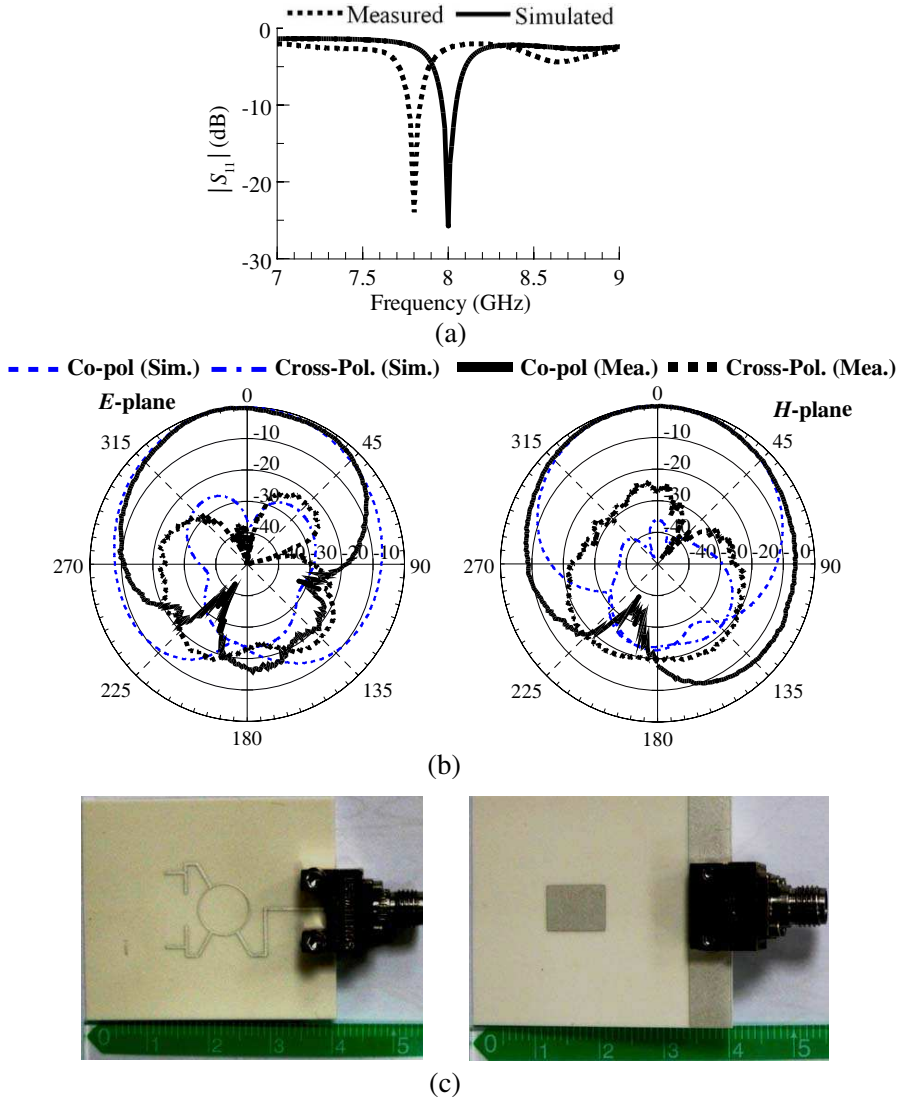


Figure 6. (a) S_{11} responses. (b) Radiation patterns, and (c) photos, of the differential probe-fed Antenna I (8 GHz).

$L = 6.8$ mm, $H_1 = 0.4$ mm, and $H_2 = 0.36$ mm. This study adopts the LTCC material system provided by Advanced Ceramic X Corporation with relative permittivity 7.5 and loss tangent 0.005. Three metal layers were used. All buried, exposed, and filled conductors were silver. This simulation used full-wave EM simulator Ansoft HFSS. A design with longer feeding probes achieves greater improvement efficiency because the cross-polarization level increases as the probe length increases. Here, thin substrates were chosen purposely to test the limit of improvement.

The measurements were conducted in a far-field anechoic chamber using the HP8510C vector network analyzer. The S_{11} , gain, and radiation patterns were measured to analyze antenna performances. The measured S_{11} curve in Fig. 6(a) shows that the central frequency shifted slightly to 7.8 GHz at a 10-dB impedance bandwidth of 1.5%. The bandwidth is narrow as a result of using thin substrates. Fig. 6(b) plots the E -plane and H -plane radiation patterns obtaining a measured gain of 3.4 dBi. The cross-polarization level remains fairly low on boresight, but increases greatly at off boresight observation angles. The measured levels of cross-polarization are low than -22.5 dB within the range of $\pm 90^\circ$. The cross-polarization performance of commercial antennas typically requires -20 dB below the peak co-polarized level. Antenna I performs better than the other differential antennas published in [1, 3, 4, 10] in terms of cross-polarization level. Fig. 6(c) shows photographs of Antenna I, with a K end-launch connector attached for testing.

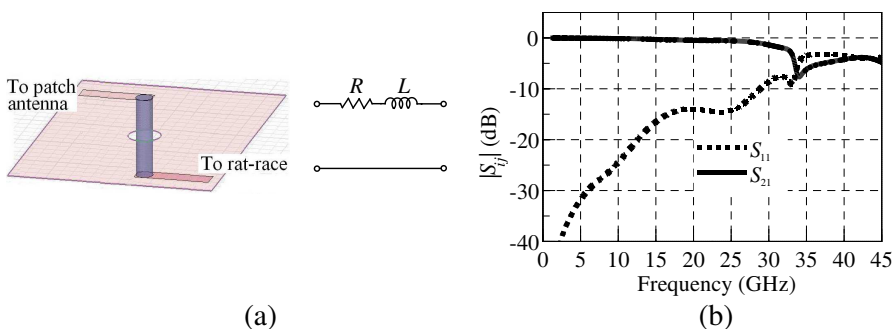


Figure 7. (a) The 3D schematic and equivalent circuit of a $50\ \Omega$ microstrip-to-microstrip vertical interconnection. (b) S -parameter frequency responses. ($H_1 = 0.4$ mm, $H_2 = 0.36$ mm, and via radius = 0.06 mm).

3.2. Differential Aperture-coupled Patch Antenna

Feeding probes may produce a large amount of parasitic inductance at high frequencies. In these cases, signal vias behave similarly to a low-pass filter, attenuating high-frequency components [13–18]. Fig. 7(a) shows the 3D schematic and the equivalent circuit of a $50\ \Omega$ microstrip-to-microstrip vertical interconnection, with $\varepsilon_r = 7.5$, $H_1 = 0.4\ \text{mm}$, $H_2 = 0.36\ \text{mm}$, and via radius = $0.06\ \text{mm}$. Fig. 7(b) plots the corresponding frequency responses of S_{11} and S_{21} , which are seriously degraded to $-9.95\ \text{dB}$ and $-1.06\ \text{dB}$ when the frequency $> 28.9\ \text{GHz}$.

Accordingly, this study proposes using a differential aperture-coupled structure, as shown in Fig. 8(a), to eliminate the parasitic inductances caused by feeding probes and improve cross-polarization at high-frequency bands. The patch and rat-race are situated on upper and lower LTCC substrates, respectively, with a ground plane in between. Two rectangular slots, parallel to the radiating edges of patches and perpendicular to the differential output arms of the rat-race, were etched on the ground plane for energy coupling. The two ground slots can also reduce the surface-wave excitation in the dielectric.

Firstly, a LTCC differential aperture-coupled patch antenna was realized at low frequency of $8\ \text{GHz}$ for preliminary test. A similar improvement of cross-polarization as Antenna I was observed. Then, a 40-GHz aperture-coupled patch antenna, Antenna II, was realized to substantiate the proof at high frequencies. Table 1 lists the detailed circuit dimensions of antennas. The patch of Antenna II measured $1.2\ \text{mm} \times 0.97\ \text{mm}$ with a substrate thicknesses of $H_1 = 0.56\ \text{mm}$ and $H_2 = 0.18\ \text{mm}$. Figs. 8(b) and 8(c) show the bottom review and top review of Antenna II, respectively, indicating the relative position of the patch, slot, and rat-race. The slots are usually $\lambda_g/4$ away from the differential open ends of the rat-race underneath the slots, where λ_g is the guided wavelength, to ensure maximum magnetic coupling. However, the accurate position should be less than $\lambda_g/4$ including the effect of open-ended capacitance. The shunt stubs of rat-race are not necessary for impedance matching. Three adjustable parameters for impedance matching are the slot length S_1 , slot width S_2 , and slot

Table 1. Physical dimensions (in mm) of the experimental antennas.

Antenna	W	L	H_1	H_2	S_1	S_2	G	d	W_l	W_r	r	L_1	L_2	L_3	L_4	L_5	L_6
I	9.09	6.8	0.4	0.36	–	–	–	–	0.44	0.21	4.05	6	3.2	3.17	1.5	4.13	8.48
II	1.2	0.97	0.56	0.18	2	0.2	1.1	0.44	0.28	0.1	0.8	–	–	–	1.08	0.83	1.68

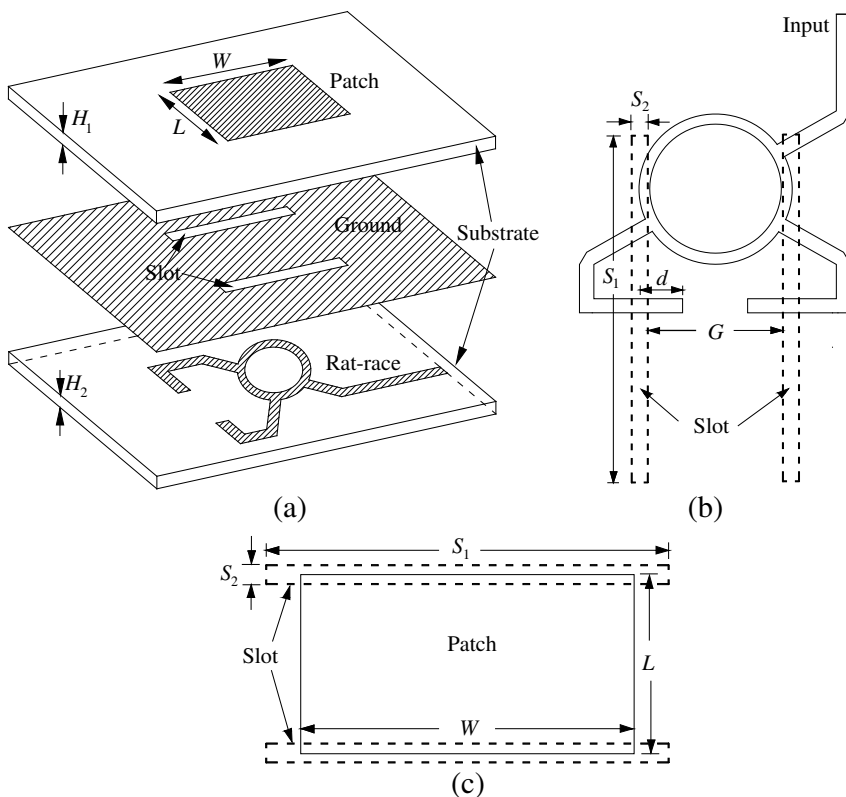


Figure 8. Proposed differential aperture-coupled patch antenna. (a) 3D schematic. (b) Bottom view. (c) Top view.

spacing G . S_1 and S_2 affect the depth of S_{11} . G primarily determines the coupling between the rat-race and the patch, and the radiation efficiency [8]. Parametric analysis reveals that an excellent return loss can be achieved when $S_1 = 2$ mm, $S_2 = 0.2$ mm, and $G = 1.1$.

Figure 9(a) shows the fine tuned S_{11} responses of Antenna II. The measured center frequency and bandwidth is 39.78 GHz and 4.7%, respectively. Simulated and measured gains were 3.6 dB and 3 dB, respectively. Fig. 9(b) shows the radiation patterns of Antenna II. The simulated cross-polarization is low than -20 dB within the range of $\pm 90^\circ$. Although part of measured cross-polarization is greater than -20 dB in some directions, it is still generally better than -15 dB. The cross-polarization level of Antenna II is lower than the antenna published in [12], but is higher than the antennas in [7, 11]. This is because the coupling aperture became very small at 40 GHz, which was difficult to realize accurately in our LTCC process. However, the level

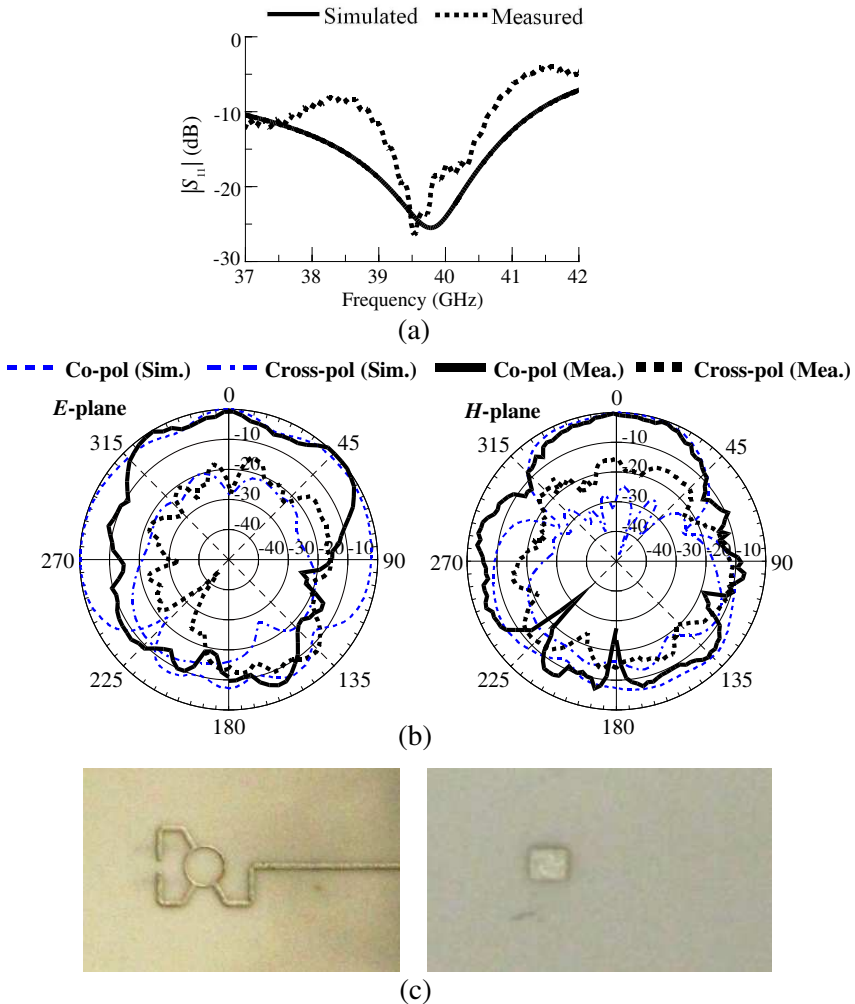


Figure 9. (a) S_{11} responses. (b) Radiation patterns, and photos, of the differential aperture-coupled Antenna II (40 GHz).

of < -15 dB is quite acceptable for practical applications. Fig. 9(c) shows photos of the 40-GHz Antenna II.

4. CONCLUSIONS

This paper proposes two feeding structures for differential patch antennas. The study also explains why an unbalanced feeding probe degrades *E*-plane co-polarization and *H*-plane cross-polarization. A differential probe-fed structure was designed to improve cross-

polarization, allowing for easy impedance matching. Antenna I was developed on LTCC substrate at 8 GHz. A low cross-polarization of less than -22.5 dB was achieved. This study further proposes using a differential aperture-coupled structure to eliminate the parasitic inductance caused by feeding probes at high-frequency bands. Antenna II was realized at 40 GHz for demonstration. The proposed design achieves a performance improvement similar to probe-fed antennas.

ACKNOWLEDGMENT

This work was partially supported by the National Science Council, Taiwan, R.O.C., (NSC 100-2221-E-182-060), the High Speed Intelligent Communication (HSIC) Research Center, and the Healthy Aging Research Center (HARC), Chang Gung University.

REFERENCES

1. Petosa, A., A. Ittipiboon, and N. Gagnon, "Suppression of unwanted probe radiation in wideband probe-fed microstrip patches," *Electron. Lett.*, Vol. 35, 355–357, Mar. 1999.
2. Zhang, Y.-P. and J.-J. Wang, "Theory and analysis of differentially-driven microstrip antennas," *IEEE Trans. on Antennas and Propagat.*, Vol. 54, No. 4, 1092–1099, 2006.
3. Xue, Q., X.-Y. Zhang, and C.-H. K. Chin, "A novel differential-fed patch antenna," *IEEE Antennas Wireless Propagat. Lett.*, Vol. 5, 471–474, 2006.
4. Li, P., H. W. Lai, K. M. Luk, and K. L. Lau, "A wideband patch antenna with cross-polarization suppression," *IEEE Antennas Wireless Propagat. Lett.*, Vol. 3, 211–214, 2004.
5. Valavan, S. E., A. B. Yang, A. Yarovoy, and L. P. Ligthart, "An M-band differentially fed, aperture coupled stacked patch antenna in LTCC," *Proceedings of the 5th European Radar Conference*, 200–203, 2008.
6. Wu, T., Y. Li, S.-X. Gong, and Y. Liu, "A novel low RCS microstrip antenna using aperture coupled microstrip dipoles," *Journal of Electromagnetic Waves and Applications*, Vol. 22, No. 7, 953–963, 2008.
7. Lee, E., K. M. Chan, P. Gardner, and T. E. Dodgson, "Active integrated antenna design using a contact-less, proximity coupled, differentially fed technique," *IEEE Trans. on Antennas and Propagat.*, Vol. 55, No. 2, 267–276, 2007.

8. Akkermans, J. A. G., M. H. A. J. Herben, and M. C. van Beurden, "Balanced-fed planar antenna for millimeter-wave transceivers," *IEEE Trans. on Antennas and Propagat.*, Vol. 57, No. 10, 2871–2881, Oct. 2009.
9. Ma, Q., B.-H. Sun, J.-F. Li, and Q.-Z. Liu, "A differential rectangular patch antenna with Marchand balun for UWB applications," *Journal of Electromagnetic Waves and Applications*, Vol. 23, No. 1, 49–55, 2009.
10. Chen, Z. N. and M. Y. W. Chia, "A novel center-slot-fed suspended plate antenna," *IEEE Trans. on Antennas and Propagat.*, Vol. 51, 1407–1410, Jun. 2003.
11. Brauner, T., R. Vogt, and W. Bächtold, "A differential active patch antenna element for array applications," *IEEE Microw. Wireless Compon. Lett.*, Vol. 13, 161–163, Apr. 2003.
12. Chan, K. M., E. Leef, P. Gardner, and P. S. Hall, "Non-contact coupling between antenna and circuit front-ends," *The 2nd European Conference on Antennas and Propagation, EuCAP*, 2007.
13. Chin, K.-S., H.-T. Chang, and J.-A. Liu, "Design of LTCC wideband patch antenna for LMDS band applications," *IEEE Antennas Wireless Propagat. Lett.*, Vol. 9, 1111–1114, 2010.
14. Xia, L., R.-M. Xu, and B. Yan, "LTCC interconnect modeling by support vector regression," *Progress In Electromagnetics Research*, Vol. 69, 67–75, 2007.
15. Chin, K.-S., H.-T. Chang, J.-A. Liu, B.-G. Chen, J.-C. Cheng, and J. S. Fu, "Stacked patch antenna array on LTCC substrate operated at 28 GHz," *Journal of Electromagnetic Waves and Applications*, Vol. 25, No. 4, 527–538, 2011.
16. Wang, Z., P. Li, R.-M. Xu, and W. Lin, "A compact X-band receiver front-end module based on low temperature co-fired ceramic technology," *Progress In Electromagnetics Research*, Vol. 92, 167–180, 2009.
17. Lee, Y. C., "CPW-to-stripline vertical via transitions for 60 GHz LTCC SoP applications," *Progress In Electromagnetics Research Letters*, Vol. 2, 37–44, 2008.
18. Cao, W.-Q., B.-N. Zhang, A. J. Liu, D.-S. Guo, T.-B. Yu, and Y. Wei, "A dual-band microstrip antenna with omnidirectional circularly polarized and unidirectional linearly polarized characteristics based on metamaterial structure," *Journal of Electromagnetic Waves and Applications*, Vol. 26, Nos. 2–3, 274–283, 2012.